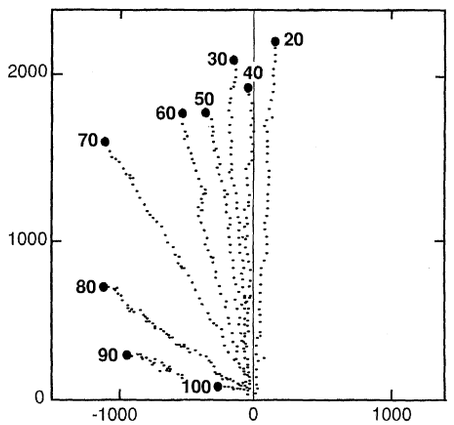

Fig. 6. Computer simulation of continuous-rotation gel electrophoresis. Nine simulated molecules ranging in size from 20 to 100 beads were started at the origin. Their paths were traced (dotted lines) for 50 revolutions of the electric field. The electric field rotated constantly with a period of 200 while the strength of the field was switched each half revolution between a value of 7 and 3. The axes are labeled with distance in units of maximal bead spacings, which, when compared with actual DNA contour length, correspond to 3 μm. This simulation ran 10 hours on an IBM PC/AT computer (*11*).

circular gel rotates continuously in a fixed-direction electric field. The mechanical setup is similar to Southern's (*3*), but instead of tacking between two fixed angles, the gel rotates at a constant rate and the electric field is switched between a high and low value every half revolution. The pattern of DNA migration, starting from three point sources, is shown in Fig. 5. The average direction of the electric field over time is straight up; it is in this direction that small DNA fragments travel (long streaks). The unexpected asymmetry of the pattern is caused by differences in the realignment rates of the molecules recently exposed to strong or weak fields. This characteristic pattern has been duplicated in tube-model simulations (Fig. 6). The simulation gives the correct lobe shape, that is, the correct angles and distances for the same relative size molecules. The model behaves correctly for different gel rotation rates, including the production of minor lobes at greater rates. Attempts are now being made to reproduce the resolving properties of field-inversion gel electrophoresis (*2*).

With readily available equipment, we have made observations of individual strands of DNA undergoing electrophoresis in pulsed and constant electric fields. Our images bear remarkable resemblance to simulations based on independently developed models. Investigations directed toward improving separations of large DNA strands are expected to advance rapidly with these new experimental techniques. A videocassette recording showing molecular motion is available for education and research (*12*).

REFERENCES AND NOTES

1. D. C. Schwartz and C. R. Cantor, *Cell* **37**, 67 (1984).
2. G. F. Carle *et al.*, *Science* **232**, 65 (1986).
3. E. M. Southern, R. Anand, W. R. A. Brown, D. S. Fletcher, *Nucleic Acids Res.* **15**, 5925 (1987).
4. L. S. Lerman and H. L. Frisch, *Biopolymers* **21**, 995 (1982); O. J. Lumpkin and B. H. Zimm, *ibid.*, p. 2315; O. J. Lumpkin, P. Dejardin, B. H. Zimm, *ibid.* **24**, 1575 (1985); G. W. Slater and J. Noolandi, *ibid.*, p. 2181.
5. J. M. Deutsch, *Science* **240**, 922 (1988).
6. H. Hervet and C. P. Bean, *Biopolymers* **26**, 727 (1987); M. Jonsson, B. Akerman, B. Norden, *ibid.* **27**, 381 (1988).
7. M. Yanagida, Y. Hiraoka, I. Katsura, *Cold Spring Harbor Symp. Quant. Biol.* **47**, 177 (1982).
8. F. Bueche, *Physical Properties Of Polymers* (Interscicence, New York, 1962).
9. G. F. Carle and M. V. Olson, *Methods Enzymol.* **155**, 468 (1987).
10. G. Chu, D. Vollrath, R. W. Davis, *Science* **234**, 1582 (1986).
11. A Pascal source code printout is available on request.
12. VHS cassettes entitled "Individual DNA Molecules Undergoing Gel Electrophoresis" can be obtained from Instructional Media Services, SB-54, University of Washington, Seattle, WA 98195.

13. We thank B. Shapiro for lending us his image intensifier.

16 August 1988; accepted 18 October 1988

Correct Folding of Circularly Permuted Variants of a βα Barrel Enzyme in Vivo

KAROLIN LUGER, ULRICH HOMMEL, MARZELL HEROLD, JAN HOFSTEENGE, KASPER KIRSCHNER*

An important question in protein folding is whether the natural amino and carboxyl termini and the given order of secondary structure segments are critical to the stability and to the folding pathway of proteins. Here it is shown that two circularly permuted versions of the gene of a single-domain βα barrel enzyme can be expressed in *Escherichia coli*. The variants are enzymically active and are practically indistinguishable from the original enzyme by several structural and spectroscopic criteria, despite the creation of new termini and the cleavage of a surface loop. This novel genetic approach should be useful for protein folding studies both in vitro and in vivo.

THE THREE-DIMENSIONAL STRUCTURE of a native protein is determined by its amino acid sequence (*1*), but it is unknown why and how a given polypeptide chain folds (*2*). From the comparison of the structures of homologous single-domain proteins and from reassembly studies with protein fragments, it appears that secondary structure segments that make up the internal core of a protein—and not the surface loops—are responsible for its stability (*3, 4*). One view of the folding mechanism envisages multiple routes involving partially folded intermediates with local nativelike structure (*5*). These folded regions are thought to consist mainly of secondary structure segments that are adjacent in the sequence.

Kinetic studies of the folding of mutant or homologous sequences have contributed importantly toward understanding protein folding (*2*). A more radical perturbation of the sequence is to rearrange the order of secondary structure segments by circular permutation; that is, by linking the natural amino and carboxyl termini through a new peptide bond and by cleaving one of the existing surface loops to create new termini. The sequence of bovine pancreatic trypsin inhibitor was the first to be permuted circularly by chemical condensation and limited proteolysis (*6*). However, this approach is not readily applicable to other proteins. It also provides no information on protein folding in vivo. We propose that circular permutation of the corresponding structural gene is a specific and versatile approach for varying the connectivity of secondary structure segments in a systematic manner and for producing the corresponding protein variants in bacteria. To demonstrate the feasibility of this novel approach, we constructed two different circular permutations of the structural gene. These genes were expressed in *Escherichia coli*, and the corresponding proteins were purified to homogeneity. Several structural and functional properties of these circularly permuted proteins show that they fold to a compact structure that is similar to that of the wild-type enzyme.

The structure of phosphoribosyl anthranilate isomerase from *Escherichia coli* (ePRAI), which is part of a bifunctional enzyme, has

K. Luger, U. Hommel, M. Herold, K. Kirschner, Abteilung Biophysikalische Chemie, Biozentrum der Universität Basel, Klingelbergstrasse 70, CH-4056 Basel, Switzerland.
J. Hofsteenge, Friedrich Miescher Institut, P.O. Box 2543, CH-4002 Basel, Switzerland.

*To whom correspondence should be addressed.

been elucidated recently (7). It is an eightfold βα barrel, a folding pattern that has been found in at least 13 other enzymes (*8*). The structure of the monofunctional, monomeric enzyme from *Saccharomyces cerevisiae* (yPRAI) is not known, but both ePRAI and yPRAI can be assumed to have the same general fold since they show 30% sequence identity (*9*). The active site of ePRAI is located at the carboxyl terminal end of the central β barrel (7). As shown by the alignment of another eight homologous sequences with those of ePRAI and yPRAI, this assignment is probably true for all species. A variant of yPRAI, which has five additional amino acids added to its original amino terminus [extended yPRAI (xPRAI)] (Fig. 1, A and C), can be expressed in *E. coli*. Since its catalytic properties are similar to those of ePRAI and yPRAI (Table 1), the active sites must also be similar and the extension of the amino-terminus does not affect correct folding.

The structure of xPRAI is probably that of a "limit βα barrel," which has no additional secondary structure segments either preceding β strand 1 or following α helix 8. The βα barrel structure fulfills the two main preconditions for the construction of a stable circularly permuted protein: (i) the carboxyl and amino termini are in close proximity (that is, predisposed for covalent linkage), and (ii) each of the 15 surface loops could be cleaved to create the new termini. Several catalytic amino acid residues are located on various β strands. Therefore, enzyme activity measurements (*10, 11*) should be a sensitive probe for the correct arrangement of these secondary structure segments.

Two different surface loops were chosen for creating new amino and carboxyl termini to test whether protein folding is affected by the particular mode of circular permutation. Both variants have the original protein termini joined by the same new oligopeptide loop (Fig. 1, B and D). cPRAI-1 is opened at the loop between α helix 6 and β strand 7, which is opposite to the active site. cPRAI-2 is opened at the loop between β strand 6 and α helix 6, which is at the active site, and also contains two conserved residues (Gly^{150} and Gly^{152} (7)). The lengths of both loops vary widely among the ten known sequences of PRAI. The sequences of the new oligopeptide joining the original protein termini and of the additions to the new termini are not unreasonable choices in terms of preferred surface location and chain flexibility (*12*).

The following describes briefly the steps leading to the structural gene of cPRAI-1. Subcloning the *TRP*-1 gene (*13*) into a vector allowing high expression in *E. coli* required the generation of a unique BAM HI restriction site to give xPRAI (Fig. 2, A and B). The introduction of two further restriction sites with matching 5′ protruding ends permitted the stepwise rearrangement that led to the coding sequence for cPRAI-1 (Fig. 2, C to E). The gene for cPRAI-2 was constructed analogously (Fig. 3, B to E).

xPRAI, cPRAI-1, and cPRAI-2 were produced in *E. coli* at high levels after transformation with the corresponding expression plasmids. In all cases, after centrifugation of the disrupted cells, about 10% of the PRAI activity was found in the supernatant and 90% was found in the pellet after reconstitution. The three enzymes were purified from the corresponding pellets as follows. The insoluble proteins were dissolved in 3*M*

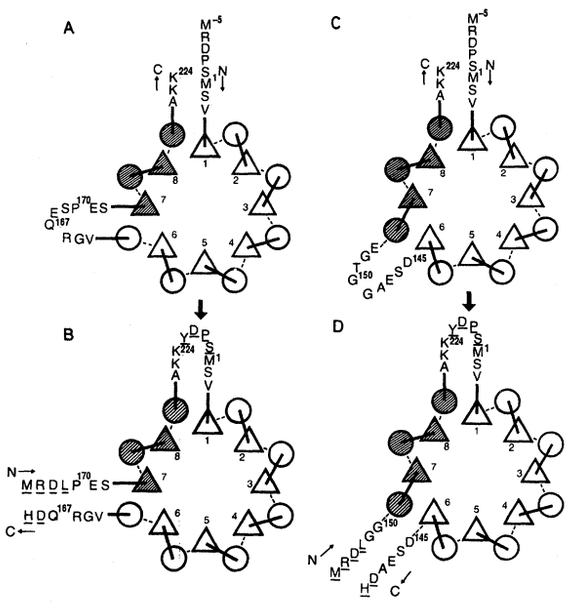

Fig. 1. Schematic representation of the eightfold βα-barrel folding pattern of xPRAI, cPRAI-1, and cPRAI-2. Triangles represent β strands, numbered in sequential order from the amino-terminus (N), perpendicular to the plane of the page, and running downward (*26*). Circles are perpendicular α helices coming upward, numbered as the preceding β strands. Connections from α to β are shown as bold lines and from β to α as dashed lines. C, carboxyl terminus. Secondary structure regions that were transferred to yield the circularly permuted proteins are shaded. (**A** and **C**) xPRAI. Partial sequences are given of the amino and carboxyl termini and of the loops (A) between α helix 6 and β strand 7, and (C) between β strand 6 and α helix 6. (**B**) cPRAI-1. Four new amino acid residues (underlined) were introduced to connect the original amino and carboxyl termini. New termini were generated by cleavage of the loop joining α6 and β7 and by addition of extra residues (underlined). (**D**) cPRAI-2. The original termini were connected as in cPRAI-1 [compare with (B)]. New termini were generated by cleavage of the loop joining β6 and α6, and addition of extra residues (underlined). Abbreviations for the amino acid residues are as follows: A, Ala; D, Asp; E, Glu; G, Gly; H, His; K, Lys; L, Leu; M, Met; P, Pro; Q, Gln; R, Arg; S, Ser; T, Thr; V, Val; and Y, Tyr.

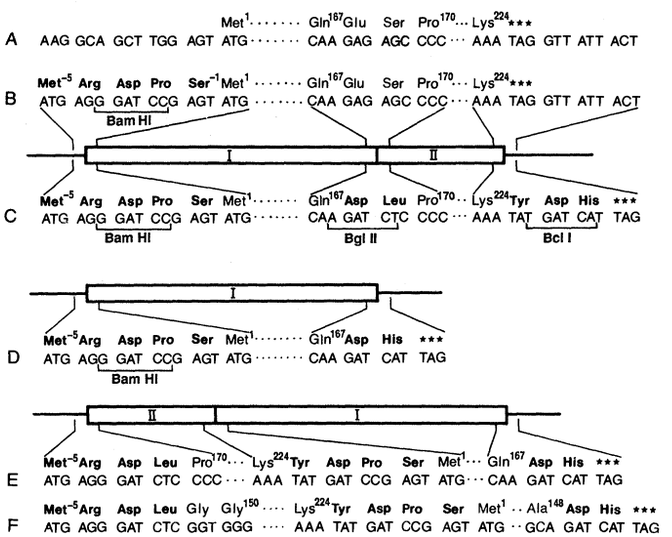

Fig. 2. Construction of the gene encoding cPRAI-1. Partial amino acid and DNA sequences; numbering of wild-type yPRAI (*13*). New amino acids are shown in bold type. New restriction sites are indicated by brackets. (**A**) yPRAI and the *TRP*-1 gene (*13*), contained in the vector pMA (*27*). (**B**) Introduction of a new Bam HI site allowed expression of the *TRP*-1 gene in the ATG expression vector pDS 56/RBSII-1 (*28*), resulting in xPRAI. (**C**) Further modification introduced new Bgl II and Bcl I restriction sites, thus leading to substitutions in the loop between α helix 6 and β strand 7 and at the carboxyl terminus (compare with Fig. 1B). (**D**) Excision of fragment II and subsequent religation of the remaining plasmid generated fragment I in an expressible form. (**E**) Insertion of fragment II into the Bam HI site of plasmid D1 in the correct orientation generated the coding sequence for cPRAI-1. (**F**) The coding sequence of cPRAI-2 that was constructed analogously to the coding sequence of cPRAI-1 (A to E). New restriction sites were introduced by oligonucleotide-directed mutagenesis, with the use of the vector pMAC (*27, 29*). Ligated DNA regions were confirmed by sequence analysis (*30*).

guanidinium chloride (GuCl) and subsequently refolded by dialysis against buffer. Each renatured enzyme was purified further by chromatography on an anion-exchange column. As judged from gel electrophoresis in the presence of SDS, each protein was more than 98% pure. The amino termini of refolded cPRAI-1 and cPRAI-2 were sequenced by the automated Edman method (*14*) to provide an identity check by an independent method. The observed sequences (MRDLPESL. . . and MRD-LG GT. . .) agreed with the expected sequences (compare Fig. 2, E and F). Native cPRAI-1 was purified partially from the supernatant to provide for a standard protein that had not passed through a cycle of aggregation, unfolding, and refolding. yPRAI was purified for comparative purposes from an overproducing strain of yeast (*15*).

Refolded xPRAI, cPRAI-1, and cPRAI-2 are monomers of the expected molecular weights (M_r ~25,000) and have similar Stokes' radii, as assessed by equilibrium ultracentrifugation and gel filtration. The ultraviolet (UV) absorption, fluorescence emission (excitation at 280 nm), and far-UV circular dichroism (CD) spectra of these proteins were practically identical (Figs. 4, 5, and 6). Thus all three proteins appear to be folded compactly and in a similar manner.

Steady-state kinetic analysis of the various forms of PRAI was performed to compare the properties of the corresponding active sites (*10, 15*) (Table 1). xPRAI rather than yPRAI is the relevant standard of comparison because it has the same four amino-terminal residues and has been expressed and purified exactly as the two circularly permuted variants.

The important results are as follows. (i) Both circularly permuted variants are enzymically active. The data in Table 1 show that cPRAI-1 has practically the same rate constant (k_{cat}) and Michaelis constant (K_m) values as ePRAI, yPRAI, and xPRAI. Thus the structures of the corresponding active sites must be similar. cPRAI-2 is also enzymically active. However, because the K_m value is at least 400-fold greater than that of xPRAI, only the value of k_{cat}/K_m was measured accurately. The value of k_{cat} is about 30-fold smaller than that of xPRAI. (ii) cPRAI-1, which had been purified from the soluble fraction to about 50% purity, had the same K_m value as cPRA-1 purified to homogeneity from the pellet. This observa-

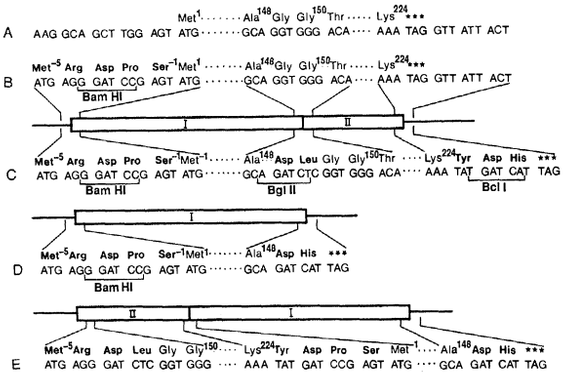

Fig. 3. Construction of the gene encoding cPRAI-2. The partial amino acid and DNA sequences of all intermediates between yPRAI and cPRAI-2 are given in the same format as Fig. 2.

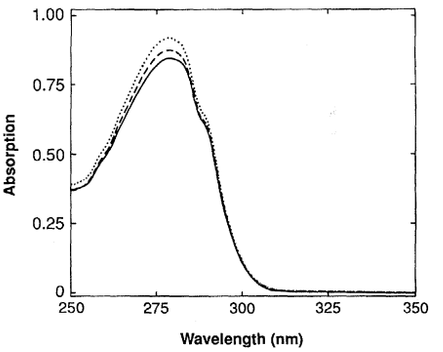

Fig. 4. Ultraviolet absorption spectra of xPRAI, cPRAI-1, and cPRAI-2. The three native proteins were dialyzed against 0.05*M* potassium phosphate buffer, *p*H 7.5, containing 1 m*M* EDTA. Each protein solution was adjusted to about 1 mg of protein per milliliter and to the same absorption at the maximum of the peptide bond absorption [λ = 230 nm, optical path length (*d*) = 1 cm]. The slightly increased absorption at 278 nm of cPRAI-1 and cPRAI-2 with respect to xPRAI is probably due to the additional Tyr residue in the oligopeptide loop that connects the original amino and carboxyl termini (compare with Fig. 1, B and D). Solid line, xPRAI; dashed line, cPRAI-1; dotted line, cPRAI-2.

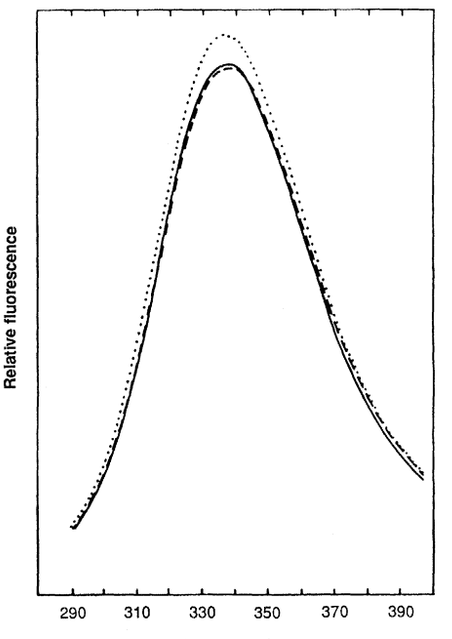

Fig. 5. Fluorescence emission spectra of xPRAI, cPRAI-1, and cPRAI-2. Fluorescence of the same preparations that were used for the measurements in Fig. 4 was excited at 280 nm in 1-cm² cuvettes. Protein concentration diluted to 0.1 mg per milliliter with the buffer described in Fig. 4. Lines are as described in Fig. 2.

Table 1. Steady-state and refolding kinetics of purified xPRAI, cPRAI-1, and cPRAI-2 (*24*). The assay was performed at 25°C in 50 m*M* tris-HCl buffer, *p*H 7.5. The labile substrate phosphoribosyl anthranilate (PRA) was generated from anthranilate and phosphoribosyl pyrophosphate in the cuvette by the phosphoribosyl transferase–catalyzed reaction (*11*). The disappearance of PRA was monitored fluorimetrically. The K_m and k_{cat} values (with SE) were generally determined by analysis of entire progress curves, but only initial velocities were measured for cPRAI-2. Refolding was initiated by 200-fold dilution of 2 mg of protein per milliliter in 4*M* GuCl with 0.05*M* potassium phosphate buffer, *p*H 6.5, containing 0.1*M* KCl, 0.02*M* dithioerythritol (DTE), and 0.01*M* K_2Mg-EDTA, at 20°C. Refolding was monitored by fluorescence emission at 320 nm (excitation at 280 nm). k_{obs}, observed first-order-rate constant.

PRA isomerase variants	Steady-state constants			Slow refolding rate constants
	k_{cat} (s^{-1})	K_m (μM)	k_{cat}/K_m ($\mu M^{-1}\ s^{-1}$)	$10^3 \times k_{obs}$ (s^{-1})
	Wild-type PRAI			
cPRAI (*11*)	40 ± 4	5.0 ± 0.8	8.0	
yPRAI (*15*)	50 ± 5	4.0 ± 0.6	12.5	
xPRAI (Fig. 1, A and C)	79 ± 8	3.7 ± 0.6	21.3	3.5 ± 0.2
	Circularly permuted xPRAI			
cPRAI-1 (Fig. 1B)*		4.6 ± 0.7		
cPRAI-1 (Fig. 1B)†	59 ± 6	5.5 ± 0.9	10.7	1.7 ± 0.1
cPRAI-2 (Fig. 1D)†	>2	>2000	0.001	2.2 ± 0.2

*Purified from the soluble fraction. †Refolded in vitro.

tion indicates that the products of in vivo and in vitro folding are identical in this case.

The new oligopeptide that connects the original amino and carboxyl termini of both cPRAI-1 and cPRAI-2 contains two Lys and one Asp residue (compare with Fig. 1, B and D) and is thus potentially susceptible to the action of trypsin or V8-protease. However, neither xPRAI, cPRAI-1, or cPRAI-2 were attacked by these proteases, as judged by their unaltered enzymic activities and mobilities during gel electrophoresis in the presence of SDS. These data show not only that the new loop in both cPRAI-1 and cPRAI-2 is inaccessible to the proteases, but also that the two structures are as compact as the parent structure of xPRAI. Thus the lower k_{cat}/K_m value of cPRAI-2 must be caused mainly by the modification of the loop between β strand 6 and α helix 6.

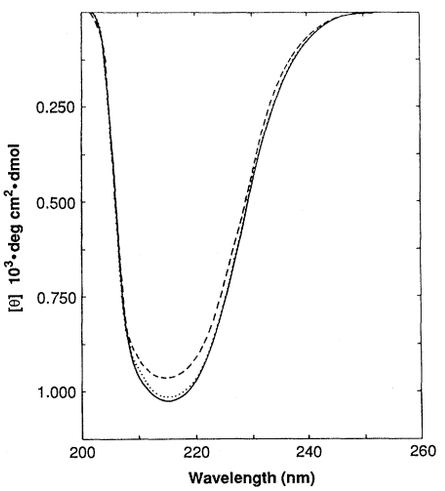

Fig. 6. Far-ultraviolet circular dichroism spectra of xPRAI, cPRAI-1, and cPRAI-2. The same preparations that were used for the measurements in Fig. 4 were scanned in d = 0.1-cm cuvettes. Protein concentration diluted to 0.7 mg per milliliter with the buffer described in Fig. 4. Lines are as described in Fig. 2.

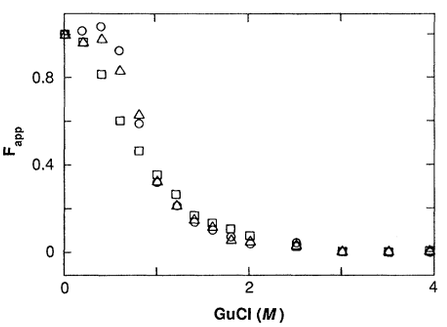

Fig. 7. Reversible unfolding of xPRAI, cPRAI-1, and cPRAI-2. Unfolding studies were performed in 50 m*M* potassium phosphate buffer, *p*H 7.5, containing 5 m*M* EDTA, 5 m*M* DTE, and the concentrations of GuCl as indicated. Protein concentrations, 0.7 mg of protein per milliliter. Protein unfolding was measured by monitoring the circular dichroism at 222 nm (θ_{222}) in 0.1-cm cuvettes. The linear change of θ_{222} above 3*M* concentration of GuCl was extrapolated to zero GuCl concentration. F_{app} is the apparent normalized deviation from this base line, averaged from four independent experiments each. ○, xPRAI; □, cPRAI-1; △, cPRAI-2.

xPRAI, cPRAI-1, and cPRAI-2 unfold reversibly in GuCl, as shown by the successful purification of these proteins from the insoluble cell fraction. At equilibrium, the unfolding curves of xPRAI, cPRAI-1, and cPRAI-2 were moderately cooperative and asymmetric (Fig. 7). The transition midpoints were at 0.88*M* (xPRAI), 0.76*M* (cPRAI-1), and 0.88*M* (cPRAI-2) GuCl. The overall unfolding transitions of xPRAI and cPRAI-2 are practically indistinguishable, but that of cPRAI-1 is less cooperative. The rates of refolding were measured to detect qualitative differences in the respective folding behavior. The progress curves were observed by fluorescence spectroscopy, and consisted of both a rapid [half-time ($t_{1/2}$) < 1 s] and a slow phase. The latter phase was fitted to a single exponential. As seen in Table 1 the rate constants of the slow refolding step vary only twofold among xPRAI, cPRAI-1, and cPRAI-2.

This work demonstrates that circularly permuted proteins can be expressed from the corresponding circularly permuted genes in *E. coli*. The three-dimensional structures of the two mutant proteins are similar to those of the wild-type protein as judged by a number of independent criteria: UV, fluorescence and CD spectroscopy; gel filtration; sedimentation; resistance towards proteases; and folding equilibria and rates. The only major difference, the lower enzymic activity of cPRAI-2, was expected, since the opened loop is at the active site and contains two conserved amino acid residues.

These results add to our understanding of protein folding. First, neither the original amino and carboxyl termini, nor the two surface loops that were cut in the process of circular permutation, are essential for finding a pathway to the stable folding pattern of xPRAI. Second, the results are most easily explained by the existence of multiple folding pathways (*5*) in which the same overall structure arises by the interaction of folding units that consist of neighboring secondary structure segments. Regions such as $\beta_7\alpha_7\beta_8\alpha_8$ or $\alpha_6\beta_7\alpha_7\beta_8\alpha_8$, which were rearranged in cPRAI-1 and cPRAI-2, respectively, are analogous to the carboxyl terminus of the α subunit of tryptophan synthase (*16*). This protein also has an eightfold βα barrel folding pattern (*17*), and the region $\alpha_6\beta_7\alpha_7\beta_8\alpha_8$ appears to fold and unfold independently (*18, 19*). Third, the results also support the "thermodynamic hypothesis" (*1*), which views protein structures as minimal free energy states.

Have circular permutations occurred during the evolution of certain proteins? Concanavalin A is not a relevant example, because circular permutation occurs posttranslationally (*20, 21*). However, about 30% of the presently known protein domains have adjacent amino and carboxyl terminal regions (*22*) and could therefore have been circularly permuted in vivo by tandem gene duplication, fusion, and deletion (*23*). Whereas examples of naturally permuted genes are expected to be found in the future, directed circular permutation should be valuable for the construction of variants for protein-folding studies both in vitro and in vivo.

REFERENCES AND NOTES

1. C. B. Anfinsen and H. C. Scheraga, *Adv. Protein Chem.* **29**, 205 (1975).
2. R. Jaenicke, *Prog. Biophys. Mol. Biol.* **49**, 117 (1987).
3. A. V. Finkelstein and O. B. Ptitsyn, *ibid.* **50**, 171 (1988).
4. M. E. Goldberg, *Trends Biochem. Sci.* **10**, 388 (1985).
5. S. C. Harrison and R. Durbin, *Proc. Natl. Acad. Sci. U.S.A.* **82**, 4028 (1985).
6. D. P. Goldenberg and T. E. Creighton, *J. Mol. Biol.* **165**, 407 (1983).
7. J. P. Priestle *et al.*, *Proc. Natl. Acad. Sci. U.S.A.* **84**, 5690 (1987).
8. C. Cothia, *Nature* **333**, 598 (1988).
9. C. Cothia and A. M. Lesk, *EMBO J.* **5**, 823 (1986).
10. K. Kirschner, H. Szadkowski, T. S. Jardetzky, V. Hager, *Methods Enzymol.* **142**, 386 (1987).
11. U. Hommel, A. Lustig, K. Kirschner, *Eur. J. Biochem.*, in press.
12. P. A. Karplus and G. E. Schulz, *Naturwissenschaften* **72**, 212 (1985).
13. G. Tschuemper and J. Carbon, *Gene* **10**, 157 (1980).
14. R. M. Hewick, M. W. Hunkapiller, L. E. Hood, W. Dreyer, *J. Biol. Chem.* **256**, 7990 (1981).
15. G. Braus *et al.*, *ibid.* **263**, 7868 (1988).
16. W. Higgins, T. Fairwell, E. W. Miles, *Biochemistry* **18**, 4827 (1979).
17. C. C. Hyde, S. A. Ahmed, E. A. Padlan, E. W. Miles, D. R. Davies, *J. Biol. Chem.* **263**, 17857 (1988).
18. E. W. Miles, K. Yutani, K. Ogasahara, *Biochemistry* **21**, 2586 (1982).
19. T. M. Stackhouse, J. J. Onuffer, C. R. Matthews, S. A. Ahmed, E. W. Miles, *ibid.* **27**, 824 (1988).
20. G. N. Reeke, Jr., and J. W. Becker, *Science* **234**, 1108 (1986).
21. D. J. Bowles *et al.*, *J. Cell. Biol.* **102**, 1284 (1987).
22. J. M. Thornton and B. L. Sibanda, *J. Mol. Biol.* **167**, 443 (1983).
23. B. A. Cunningham, J. J. Hemperly, T. P. Hopp, G. M. Edelman, *Proc. Natl. Acad. Sci. U.S.A.* **76**, 3218 (1979).
24. Purification of xPRAI, cPRAI-1, and cPRAI-2 from *E. coli* strain SG 200-50 (strain collection of D. Stueber) harboring the corresponding expression plasmid (compare with Fig. 2, B, E, and F), were induced at an optical density at 600 nm of 0.4 with 1 m*M* final concentration of isopropylthiogalactoside (*25*) and cultivated for another 5 hours (xPRAI) or 2.5 hours (cPRAI-1 and cPRAI-2) at 37°C in Luria broth medium. Cells were opened by sonication at 0°C in buffer C [0.1*M* potassium phosphate, *p*H 7.5, 2 m*M* EDTA, 2 m*M* DTE, 0.1 m*M* phenylmethylsulfonyl fluoride (PMSF)] at a concentration of 1 g of wet cells per milliliter. The pellet was dissolved in 3*M* GuCl in buffer C and left at room temperature for 45 min. After centrifugation, the clear supernatant was dialyzed at 4°C against 10

mM potassium phosphate, pH 7.5, containing 2 mM EDTA, 1 mM DTE, and 0.1 mM PMSF. The precipitate was removed by centrifugation, and the supernatant containing the PRAI activity was applied to a DEAE-Sepharose fast-flow column, equilibrated with the same buffer, and eluted with a linear phosphate gradient. After addition of 10% glycerol, the pure proteins were stored at −70°C. Typically, 5 to 10 mg of protein was obtained from 1 g of wet cells.
25. U. Certa *et al.*, *EMBO J.* **5**, 3051 (1986).
26. M. J. E. K. Sternberg and J. M. Thornton, *Nature* **271**, 15 (1978).
27. P. Stanssens, personal communication.
28. D. Stueber, personal communication.
29. W. Kramer *et al.*, *Nucleic Acids Res.* **12**, 9441 (1984).
30. F. Sanger, S. Nicklen, A. R. Coulson, *Proc. Natl. Acad. Sci. U.S.A.* **74**, 5463 (1977).
31. We thank our colleagues for critical comments, P. Stanssens and D. Stueber for providing procedures, plasmids, and bacterial strains. Supported by the Swiss National Science Foundation.

8 August 1988; accepted 11 November 1988

Involvement of Juvenile Hormone in the Regulation of Pheromone Release Activities in a Moth

MICHEL CUSSON AND JEREMY N. MCNEIL*

Juvenile hormone has been implicated in the mediation of several reproduction-related events in adult insects, but had previously been found to play no role in the regulation of sex pheromone production and release behavior ("calling") in moths. In females of the true armyworm moth, *Pseudaletia unipuncta*, juvenile hormone is shown to be essential to the initiation of both calling behavior and pheromone production. Females without corpora allata, the source of juvenile hormone, do not call and do not produce pheromone, but injection of juvenile hormone into allatectomized females restored these activities. The armyworm's control system has likely evolved in response to the adults' migratory behavior which may necessitate that mating be restricted to the period following migration.

FEMALES OF MANY INSECT SPECIES attract mates by means of a sex pheromone, the release of which is frequently associated with a characteristic behavior termed "calling" (*1*). Early studies of the physiological regulation of pheromone emission indicated that the presence of corpora allata (CA), the source of juvenile hormone (JH), was essential for mate attraction in some cockroaches, but that pheromone release was unaffected by CA removal in the females of two species of moth (*2*). Subsequent investigations on other moths yielded similar results (*3, 4*). We now report that, unlike the moth species previously studied, females of the true armyworm, *Pseudaletia unipuncta* (Noctuidae), require CA in order to synthesize pheromone and express calling behavior.

After comparing the reproductive cycle of cockroaches with that of moths, Barth (*2*) proposed the hypothesis that neuroendocrine control of pheromone release activities would be expected to evolve only in insects that are long-lived as adults and in which there are periods when mating is suppressed. Unlike cockroaches, the moths that he and others examined have short adult lives and are physiologically ready to mate soon after eclosion, making the involvement of a complex endocrine control system unnecessary. In contrast with these moths, *P. unipuncta* females do not mate immediately after emergence. Instead, they delay all mating-related activities for varying lengths of time in response to environmental conditions. When they are subjected to temperatures and photoperiods that mimic those encountered in the spring or in the fall [which are thought to be associated with long-distance flights (*5*)], females initiate calling at a much older age than when they are exposed to summer-like conditions (*6*). Because migratory behavior, and the often-associated arrest in ovarian development, appear to be under the control of JH in some species of insects (*7*), we tested the hypothesis that the same hormone might play a key role in either suppressing or stimulating pheromone production and calling behavior in armyworm moths.

We have demonstrated that the brain-suboesophageal ganglion (SOG) complex of *P. unipuncta* females contains a substance with effects similar to the pheromone biosynthesis-activating neuropeptide (PBAN) discovered in *Heliothis zea* (*8*). Armyworm females that were neck-ligated during the photophase did not produce pheromone during the following scotophase (dark phase) (*9*). However, ligated females injected with a brain-SOG homogenate contained relatively large amounts of pheromone 3 hours following injection, whether the injection was performed during the scotophase or the photophase (Table 1). This indicates that the true armyworm's pheromone gland, unlike that of *H. zea* (*10*), can produce pheromone during the photophase.

We have also shown the existence of a clear relation between pheromone release activities and ovarian development in *P. unipuncta*, and we proposed two models to explain the possible involvement of JH as the factor governing the initiation of pheromone production and calling (*11*). In one model (Fig. 1A), JH acts directly on the central nervous system (CNS) to allow the release of PBAN [possibly by the corpora cardiaca (*10*)] for pheromone biosynthesis and the sending of neural messages (*4*) that initiate the expression of calling behavior. The second model (Fig. 1B) involves an intermediate hormone released by the ovary, in response to JH stimulation. We present data that support the former model.

The CA were removed (allatectomy) from newly emerged females, anesthetized under CO_2. These, along with untreated controls and sham-operated females, were observed daily during the last 1.5 hours of the scotophase to determine the age of first calling (*12*). At the end of the fifth scotophase, all females were sacrificed for pheromone titer analysis and ovarian development assessment.

More than half of the sham-operated and control females called by day 5, whereas none of the allatectomized ones did (Fig. 2A). Furthermore, allatectomized females

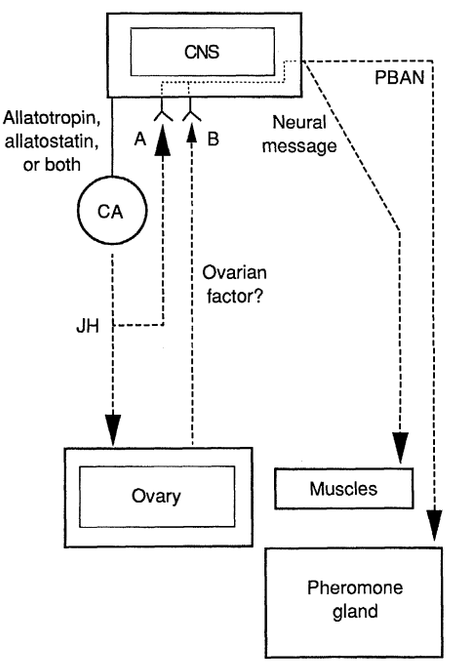

Fig. 1. Diagram illustrating the two pathways (A and B) proposed by Cusson and McNeil (*11*) to explain the role of JH in the regulation of pheromone production and calling behavior in *Pseudaletia unipuncta*.

Département de biologie, Université Laval, Sainte-Foy, Québec, Canada, G1K 7P4.

*To whom correspondence should be addressed.